Arp2/3 mediates early endosome dynamics necessary for the maintenance of PAR asymmetry in *Caenorhabditis elegans*

Jessica M. Shivas and Ahna R. Skop
Department of Genetics and Medical Genetics, University of Wisconsin–Madison, Madison, WI 53706

ABSTRACT **The widely conserved Arp2/3 complex regulates branched actin dynamics that are necessary for a variety of cellular processes. In *Caenorhabditis elegans*, the actin cytoskeleton has been extensively characterized in its role in establishing PAR asymmetry; however, the contributions of actin to the maintenance of polarity before the onset of mitosis are less clear. Endocytic recycling has emerged as a key mechanism in the dynamic stabilization of cellular polarity, and the large GTPase dynamin participates in the stabilization of cortical polarity during maintenance phase via endocytosis in *C. elegans*. Here we show that disruption of Arp2/3 function affects the formation and localization of short cortical actin filaments and foci, endocytic regulators, and polarity proteins during maintenance phase. We detect actin associated with events similar to early endosomal fission, movement of endosomes into the cytoplasm, and endosomal movement from the cytoplasm to the plasma membrane, suggesting the involvement of actin in regulating processes at the early endosome. We also observe aberrant accumulations of PAR-6 cytoplasmic puncta near the centrosome along with early endosomes. We propose a model in which Arp2/3 affects the efficiency of rapid endocytic recycling of polarity cues that ultimately contributes to their stable maintenance.**

Monitoring Editor
Francis A. Barr
University of Liverpool

Received: Jan 4, 2012
Revised: Mar 23, 2012
Accepted: Mar 23, 2012

INTRODUCTION

The generation of cell diversity in a eukaryotic organism relies on the asymmetric partitioning of cues into distinct cellular domains. The stable maintenance of these domains is necessary for many cell types to develop and function properly. The *Caenorhabditis elegans* one-celled embryo begins to polarize along the anterior–posterior axis just after fertilization (Cuenca *et al.*, 2003; Goldstein and Macara, 2007). In this system, the well-conserved PAR proteins distinguish the anterior end of the embryo from the posterior end. The anterior PAR complex, which is made up of PAR-6/PAR-3/PKC-3, localizes to the anterior cortex during the first cell cycle. PAR-2 and PAR-1 occupy the posterior cortex. The cortical domains are maintained through the rest of the cell cycle and are necessary to regulate the pulling forces that generate the asymmetric first cell division.

In *C. elegans* the formation of the PAR cortical domains occurs in two distinct phases: establishment and maintenance. The RhoA orthologue RHO-1 and the actin–myosin cytoskeleton participate in the establishment of polarity, in part by directing cortical flow (Munro *et al.*, 2004; Motegi and Sugimoto, 2006; Cowan and Hyman, 2007). The completion of the establishment phase is marked by pseudocleavage formation. CDC-42, another member of the Rho family of GTPases involved in regulating actin dynamics, is required specifically for the maintenance of cell polarity (Aceto *et al.*, 2006). The mechanism for how CDC-42 achieves this role is somewhat unclear. The widely conserved multisubunit complex Arp2/3 is crucial for the formation of branched actin networks (Goley and Welch, 2006). It associates with an existing "mother" filament and nucleates the growth of a new actin filament 70° from the existing filament (Goley and Welch, 2006). Whereas Arp2/3-mediated actin dynamics regulate polarity in many eukaryotic systems (Goley and Welch, 2006;

This article was published online ahead of print in MBoC in Press (http://www.molbiolcell.org/cgi/doi/10.1091/mbc.E12-01-0006) on March 28, 2012.

J.M.S. designed and performed all experiments and data analyses.

The authors have no conflict of interest.

Address correspondence to: Ahna R. Skop (skop@wisc.edu)

Abbreviations used: Arp, actin-related protein; CDC-42, cell division control protein 42; DYN-1, dynamin; EBP-2, end-binding protein; EEA-1, early endosome antigen 1; FYVE domain, Fab1 YOTB Vac1 and EEA1; GEX-3, gut on exterior; GFP, green fluorescent protein; NAP1/NCKAP1, Nck-associated protein; PAR, partitioning defective; PN, pronuclear; RNAi, RNA interference; WASp, Wiskott-Aldrich syndrome protein; WAVE, WASp family verprolin homologous protein; WT, wild type.

Supplemental Material can be found at:
http://www.molbiolcell.org/content/suppl/2012/03/27/mbc.E12-01-0006v1.DC1.html

Georgiou *et al.*, 2008; Leibfried *et al.*, 2008; Harris and Tepass, 2010), the contributions of Arp2/3 to the mechanisms involved in the maintenance of polarity in the *C. elegans* embryo are less clear (Severson and Bowerman, 2003; Xiong *et al.*, 2011).

It is well established that branched actin networks are required for endocytosis and recycling in budding yeast (Smythe and Ayscough, 2006; Lanzetti, 2007; Robertson *et al.*, 2009; Slaughter *et al.*, 2009). The efficient function of endocytic processes reinforces the polarization of the Cdc42p cap, which specifies the bud site in *Saccharomyces cerevisiae* (Ayscough, 2000; Irazoqui *et al.*, 2005; Marco *et al.*, 2007; Slaughter *et al.*, 2009; Orlando *et al.*, 2011). The requirements of actin in endocytosis and membrane trafficking in higher eukaryotes vary among organisms and cell types (Taunton *et al.*, 2000; Taunton, 2001; Yarar *et al.*, 2005; Kaksonen *et al.*, 2006; Smythe and Ayscough, 2006; Lanzetti, 2007; Puthenveedu *et al.*, 2010), but the endocytic pathway is emerging as a conserved mechanism necessary to stably maintain polarity in multicellular organisms (Marco *et al.*, 2007; Georgiou *et al.*, 2008; Leibfried *et al.*, 2008; Nakayama *et al.*, 2009; Shivas *et al.*, 2010). The contributions of actin to endocytic processes required for the maintenance of polarity have not been determined in the *C. elegans* embryo.

We report here that Arp2/3 is involved in the cortical localization and organization of several different factors during the polarity maintenance phase. In particular, the formation of short, punctate actin filaments is hampered upon disruption of Arp2/3 levels. Subsequently, CDC-42 accumulates at the cortex, and the stable maintenance of PAR asymmetry is disrupted. We also observe defects in the localization of endocytic proteins, including the large GTPase dynamin. Although endocytosis is not obviously affected, we observe significantly larger early endosomes and accumulations of PAR-6 in association with these enlarged endosomes. We propose that Arp2/3-mediated actin dynamics plays a key role in the regulation of early endosome dynamics and in the rapid recycling of anterior polarity cues back to the cell cortex, which promotes the stabilization of PAR asymmetry before the onset of mitosis.

RESULTS

ARX-2 is required for maintenance-phase actin dynamics

To characterize the role of the Arp2/3 complex during the first cell cycle, we used feeding RNA interference (fRNAi) to deplete the levels of the *C. elegans* Arp2 orthologue ARX-2. We examined cortical Z-series projections of embryos expressing a green fluorescent protein (GFP)–tagged fragment of moesin (GFP-moe) that labels filamentous actin (Motegi *et al.*, 2006; Velarde *et al.*, 2007). As previously reported (Velarde *et al.*, 2007), control embryos expressing this construct show a meshwork of actin filaments during the establishment phase of polarity when the embryo is contracting to generate cortical flow (Figure 1A). This meshwork retracts to the anterior half of the embryo during establishment phase. On completion of the establishment phase (pseudocleavage; Figure 1A; pronuclear [PN] meeting – 4:00 [times are in min:s]), the actin meshwork breaks down into shorter filaments and foci that remain enriched at the anterior cortex (Figure 1A, 0:00 PN meeting + 4:00; Velarde *et al.*, 2007).

In *arx-2* fRNAi-treated embryos, the actin meshwork looks similar to wild type during the polarity establishment phase (Figure 1A). However, upon entering the maintenance phase, there are fewer actin foci at the cortex (Figure 1A, 0:00). Quantification of the number of individual actin foci at PN meeting, PN meeting + 1:00, and PN meeting + 4:00 revealed a significant reduction in the number of cortical actin puncta that form over these time points. (Figure 1B; p values in legend). A similar reduction in cortical actin foci upon depletion of ARX-2 by fRNAi was previously reported (Xiong *et al.*, 2011). As the maintenance phase progresses, the foci condense to a small area of the cortex and remain there until the cell divides.

To determine whether upstream nucleation-promoting factors of Arp2/3 affected actin dynamics similarly, we depleted the WASp homologue WSP-1 and the WAVE homologue WVE-1. Depletion of either protein singly did not cause defects in actin organization (unpublished data). WVE-1 RNAi alone is only partially penetrant (Patel *et al.*, 2008), and so we instead disrupted function of the WAVE/SCAR complex by depleting GEX-3 (Xiong *et al.*, 2011). *gex-3* encodes a homologue of NAP1/NCKAP1—a ligand of the small GTPase Rac1—and has been reported to affect actin dynamics involved in cell migration and tissue morphogenesis later in *C. elegans* development (Soto *et al.*, 2002; Patel *et al.*, 2008). We found that upon depletion of GEX-3, there was a similarly significant decrease in the number of cortical actin foci at the anterior throughout the maintenance phase (Supplemental Figure S1, A and B; p values in the legend). These results are also similar to those reported previously (Xiong *et al.*, 2011). These data suggest that Arp2/3 and the WAVE/SCAR complex play a specific role in the formation and maintenance of short actin filaments and foci during the polarity maintenance phase.

ARX-2 is required for PAR-2 maintenance

In *C. elegans*, the role of actin dynamics in the maintenance of PAR asymmetry has not been well characterized. Therefore we sought to determine whether the disruption of actin foci formation would alter polarity cue localization. It was recently reported that ARX-2 affects the localization of one of the posterior PAR proteins, PAR-2, specifically during the maintenance phase of polarity (Xiong *et al.*, 2011). We reached similar conclusions using a different analysis. Cortical Z-series projections revealed that in wild-type or control embryos expressing GFP–PAR-2 (Schonegg *et al.*, 2007), PAR-2 is recruited to the posterior cortex as the posterior end of the embryo begins smoothing. On average, 43.8 ± 4.28% (n = 5 embryos) of the cortical area is occupied by GFP–PAR-2 by pseudocleavage formation (Figure 1, C and D, PN meeting – 4:00). This area decreases slightly as the embryo progresses through the maintenance phase, occupying 39.78 ± 7.57% (n = 5 embryos) of the total cortical area at pronuclear meeting and remaining steady through 4:00 min after pronuclear meeting (Figure 1C). In *arx-2* RNAi-treated embryos, the area occupied by GFP–PAR-2 appears unaffected during establishment phase; however, PAR-2 expands beyond the typical domain during the maintenance phase to occupy almost 60% of the total cortical area over the course of multiple time points (Figure 1, C and D; wild type [WT]. n = 5 embryos; *arx-2* RNAi, n = 5 embryos; p values in Figure 1D legend). However, before cell division, GFP–PAR-2 retracts back to a normal cortical domain and the embryo divides asymmetrically, likely due to a rescue mechanism that takes place during mitosis (Cai *et al.*, 2003; Siegrist and Doe, 2007; Schenk *et al.*, 2010). These data suggest that ARX-2–mediated actin dynamics and associated regulatory factors play a role in preventing PAR-2 expansion into the anterior domain during maintenance phase.

ARX-2 is required for CDC-42 down-regulation during the maintenance phase

We next examined the localization of GFP–CDC-42 due to its involvement specifically in PAR maintenance (Aceto *et al.*, 2006). CDC-42 is the *C. elegans* orthologue of Cdc42—a member of the Rho family of small GTPases that affect actin dynamics and cell polarity (Ridley, 2006). We examined the cortex by generating cortical Z-series projections of wild-type and *arx-2* RNAi embryos expressing GFP–CDC-42 (Motegi and Sugimoto, 2006). In the wild-type

embryos, CDC-42 localizes to long structures (on average, 2.54 ± 1.59 µm in length; n = 5 embryos) at the cortex that become enriched at the anterior during the establishment phase (Figure 1E, –4:00; Motegi *et al.*, 2006). CDC-42 remains anteriorly localized through maintenance phase; however, the area occupied at 4:00 after PN meeting is reduced. The foci are also significantly shorter, averaging 1.30 ± 0.69 µm in length (Supplemental Figure S2A; p values in legend). The reasons or mechanisms for the down-regulation of CDC-42 levels at the cortex or the change in size during late maintenance phase are unknown.

In *arx-2* RNAi-treated embryos, the GFP-CDC-42–labeled structures during establishment phase are shorter and more condensed than in controls, averaging 1.76 ± 1.05 µm in length (Figure 1E and Supplemental Figure S2B). CDC-42 still becomes enriched at the anterior end of the embryo and is maintained. In contrast to the controls, we observed little change in the length of the foci between establishment and maintenance phase in *arx-2* RNAi-treated embryos (1.63 ± 1.01 µm in length; Supplemental Figure S2B). In terms of the cortical area, CDC-42 occupies a greater area of the cortex 4:00 after PN meeting than in the controls (Figure 1, E and F; p values in legend; wild-type/control, n = 7 embryos; *arx-2* RNAi, n = 7 embryos), indicating that CDC-42 dynamics are significantly disrupted. These data suggest that ARX-2-mediated maintenance of polarity extends beyond the PARs, and that possibly an Arp2/3-dependent mechanism is required for the down-regulation or removal of CDC-42 from the cortex during the late stages of maintenance phase.

ARX-2 depletion causes PAR-6 accumulations near the cortex

To determine whether the appropriate localization of the anterior PAR complex also relied on Arp2/3-mediated actin dynamics, we examined GFP–PAR-6 localization in control and ARX-2–depleted embryos. As previously reported, GFPxPAR-6 localizes to the anterior cortex during the establishment phase and is maintained there (Munro *et al.*, 2004). In the *arx-2* RNAi-treated embryos, the cortical area occupied by GFP–PAR-6 was somewhat reduced during the maintenance phase; however, this was statistically significant only at the PN meeting + 1:00 time point (Figure 1, G and H), further suggesting that disruption of Arp2/3 leads to a destabilization of PAR asymmetry specifically during the maintenance phase.

We also observed GFP-PAR-6–labeled foci at or near the anterior cortex during the establishment phase and earlier portions of the maintenance phase in wild-type embryos (Figure 1G, +4:00). The nature of these puncta is unclear; however, they appear to disperse or are removed from the cortex by 4:00 after pronuclear meeting. In embryos depleted of ARX-2, these foci appear to remain at or near the cortex longer than what was observed in wild-type embryos (Figure 1G, +4:00) and formed large aggregates similar to those observed in the moe-GFP background (Figure 1A). We were interested in determining whether these GFP–PAR-6 aggregates were associated with the moe-GFP aggregates. To do so, we generated a strain expressing moe-mCherry and GFP–PAR-6. In control embryos in which a single cortical focal plane was imaged, there are instances in which GFP–PAR-6 foci overlap with or are adjacent to moe-mCherry foci during the maintenance phase (Figure 1I). At PN meeting, 39.5 ± 6.5% of the PAR-6 cortical foci were colocalized or partially colocalized with moe-mCherry foci (n = 4 embryos). By 4:00 after PN meeting, however, many of the GFP–PAR-6 foci are gone (Figure 1I). We found that the larger GFP–PAR-6 aggregates and moe-mCherry foci condensed to the same small cortical area in the *arx-2* RNAi-treated embryos (Figure 1J). These data suggest that Arp2/3 affects PAR-6 dynamics during the polarity maintenance phase.

ARX-2 does not affect microtubule contacts with the cortex during the maintenance phase

Microtubules affect cortical cell polarity in the *C. elegans* embryo (Motegi *et al.*, 2006; Ai *et al.*, 2011; Xiong *et al.*, 2011). Recently it was reported that ARX-2 depletion affected microtubules, in that the fluorescence intensity of a tubulin marker, GFP–TBA-2, was reduced at the centrosomes (Xiong *et al.*, 2011). However, it was unclear whether *arx-2* RNAi-treated embryos were actually deficient in microtubule–cortex contacts. To determine whether this was the case, we imaged a single cortical focal plane of a strain expressing EBP-2–GFP (Srayko *et al.*, 2005), a marker for the plus ends of microtubules. A single cortical focal plane was imaged, and the GFP-labeled cortical foci were counted every 5 s from PN meeting through 5:00 after PN meeting. In this analysis, we did not find significant differences in the total number of microtubule plus ends contacting the cortex in wild-type/control or *arx-2* RNAi-treated embryos. (Figure 2, A and B; p values in legend). Although there may be some subtle microtubule defects at the centrosome, the observation that the numbers of microtubule contacts with the cortex are unaffected suggests that the mislocalizations of cortical proteins are independent of microtubules.

ARX-2 is required for organization of endocytic proteins at the cortex

Owing to the disruption of the formation and organization of actin foci specifically during the polarity maintenance phase, we were interested in determining whether the cortical organization of endocytic machinery relied on ARX-2. In particular, we wanted to focus on the large GTPase dynamin. Dynamin has been extensively characterized in vesicle scission (Ferguson and De Camilli, 2012), but we were also drawn to examine its localization based on previous data suggesting its importance in the formation of actin comets and other actin-based structures (McNiven *et al.*, 2000; Merrifield *et al.*, 2002; Schafer, 2002, 2004; Krueger *et al.*, 2003; Kaksonen *et al.*, 2006; Lanzetti, 2007). As described previously, DYN-1–GFP foci localize across the cortex before the onset of polarity establishment in wild-type embryos. The foci become enriched in the anterior and are maintained through cytokinesis (Figure 2C, control; Nakayama *et al.*, 2009). In *arx-2* RNAi-treated embryos, the number of DYN-1-GFP–labeled foci at the cortex is reduced significantly (Figure 2, C and D; p values in legend). In addition, there is a reduction in the cytoplasmic background fluorescence observed. To determine whether the disruption in DYN-1–GFP foci to the cortex was specific to Arp2/3-regulated actin dynamics, we again disrupted WAVE function through *gex-3* RNAi and quantified the number of DYN-1 foci at the cortex (Figure 2, C and D). We found that disruption of WAVE/SCAR function by *gex-3* RNAi also significantly reduces the number of DYN-1–GFP cortical foci, similar to *arx-2* RNAi, suggesting that localization of DYN-1 cortex relies on Arp2/3 and WAVE/SCAR-mediated actin dynamics.

Similar to the phenotype observed in the *arx-2* RNAi treatment of moe-GFP–expressing embryos (Figure 1A), the DYN-1–GFP foci also condense in a small area of the anterior cortex during the later stages of the polarity maintenance phase (Figure 2C; PN meeting + 4:00). We next wanted to determine whether the actin foci and DYN-1–GFP foci were localizing to the same structures. To do so, we imaged a single cortical focal plane of embryos expressing DYN-1–GFP and moe-mCherry and found that 45.3 ± 4.6% of the DYN-1–GFP foci overlapped with or were adjacent to small, cortical actin filaments and puncta in wild-type embryos at PN meeting (n = 4 embryos; Figure 2D; Merrifield *et al.*, 1999; Lee and

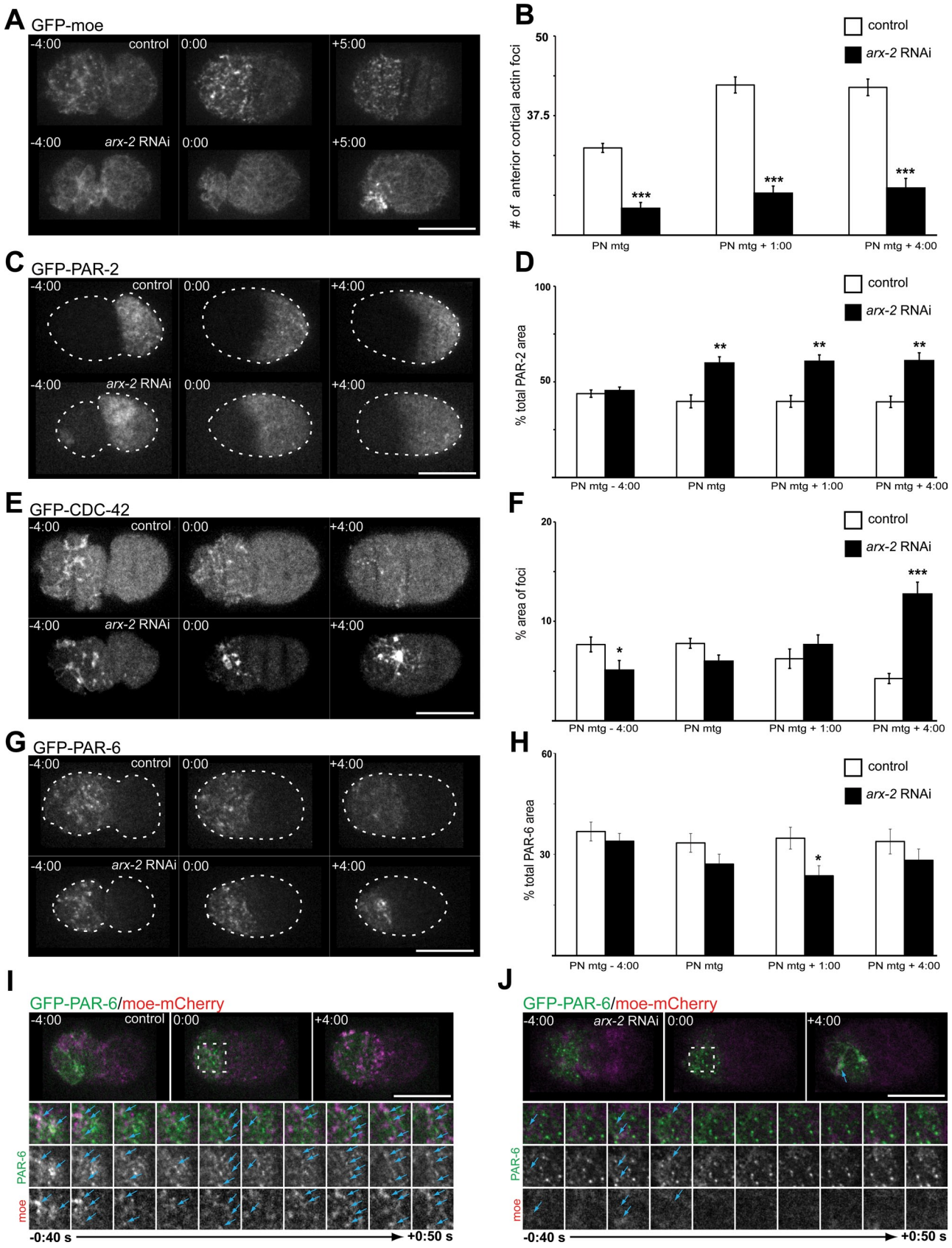

FIGURE 1: ARX-2 affects actin dynamics and polarity maintenance. (A) Projected cortical Z-series of moe-GFP–expressing wild-type embryos and embryos that were depleted of ARX-2. (B) Over the course of the maintenance phase at the time points indicated in wild-type and ARX-2–depleted embryos. Results are the mean ± SEM. p values are as follows: PN meeting, $p = 2.0 \times 10^{-6}$; PN meeting + 1:00, $p = 1.04 \times 10^{-7}$; PN meeting + 4:00, $p = 1.89 \times 10^{-6}$ (Welch's *t* test, wild-type, n = 8 embryos; *arx-2* RNAi, n = 8 embryos). (C) Cortical Z-series projections of wild-type and *arx-2*

De Camilli, 2002; Merrifield *et al.*, 2002; Nakayama *et al.*, 2009). Later in the maintenance phase (4:00 after PN meeting), 73.9 ± 6.8% of the DYN-1–GFP foci were colocalized with or adjacent to moe-mCherry–labeled foci (n = 4 embryos; Figure 2D, +4:00). In the *arx-2* RNAi-treated embryos, the larger aggregates of actin and DYN-1–GFP appear to localize to a similar area, and in some cases overlap, during the maintenance phase (Figure 2E). These data indicate that Arp2/3 is necessary to organize, and possibly recruit, dynamin to the cortex.

Owing to the reduction and disorganization of DYN-1–GFP foci at the cortex, we were interested in determining whether *arx-2* RNAi led to a disruption in clathrin levels. We generated cortical Z-series projections of wild-type or control embryos expressing GFP–CHC-1 (Sato *et al.*, 2005). In these embryos, there appeared to be little, if any, asymmetry in the localization of GFP-labeled foci (Supplemental Figure S3). In embryos depleted of ARX-2, however, there is a strong accumulation of GFP-labeled puncta at the anterior cortex (Supplemental Figure S3). We also observe more "open" puncta in *arx-2* RNAi-treated embryos than in wild-type or control embryos expressing this construct. These "open" puncta might suggest delays in the constriction of clathrin-coated pits, which has been observed in association with disruption of actin dynamics in other systems (Yarar *et al.*, 2005). We observed the strong anterior accumulation at similar time points as when we observed a decrease DYN-1 cortical puncta, which suggested a possible disruption in endocytosis.

ARX-2 does not affect membrane internalization

We next sought to determine whether the disruption in DYN-1–GFP localization to the cortex and the accumulation of GFP-labeled clathrin heavy chain correlated with a disruption in endocytosis. To do so, we assayed internalization of FM1-43, a lipophilic fluorescent dye. We previously reported that a similar dye, FM2-10, was internalized largely from the anterior membrane in a dynamin-dependent manner during the maintenance phase (Nakayama *et al.*, 2009). In a blind analysis, we found that there was no significant difference in the overall number of vesicles internalized when ARX-2 levels were decreased. There was also no difference in the asymmetry of internalization in control versus *arx-2* RNAi-treated embryos labeled with the dye (unpublished data). It is possible that depletion of Arp2/3-mediated actin dynamics does not participate in endocytosis at the internalization stage but perhaps affects the efficiency of endocytosis, which would not be reflected in our assay.

ARX-2 depletion causes cytoplasmic membrane aggregates

We previously reported close association of RAB-5–GFP, a marker for early endosomes, and actin foci in the cytoplasm of fixed *C. elegans* zygotes labeled with phalloidin (Nakayama *et al.*, 2009). We were interested in examining this association in living cells. We imaged a single, mid-focal plane of embryos expressing moe-GFP and mCherry–RAB-5 and examined the movement of endosomes relative to actin. We observed many RAB-5–positive endosomes moving away from the plasma membrane that coincided with the appearance of an actin focus (Figure 3A, times +0:56 through +1:17). Actin localized to the site of endosome entry in 94.4 ± 9.3% of the movements (n = 6 embryos). Of the endosomal entries we could detect, actin followed 58.4 ± 10.6% of the endosomes into the cell (n = 6 embryos). We also observed actin associated with endosome movement back toward the plasma membrane (Figure 3B; see also Supplemental Movie S3B). Actin was associated with the endosomes before movement back to the plasma membrane in 77.7 ± 34.4% of recycling-like events (n = 6 embryos). Finally, we could also detect what appeared to be endosomal fission events, similar to those reported in other systems (Derivery *et al.*, 2009). Actin foci were associated with 97.2 ± 6.8% of the endosomal fission events (Figure 3C and Supplemental Figure S4A, n = 7 embryos; see also Supplemental Movie S3C). Therefore these data suggest that actin dynamics can affect several aspects of early endosome dynamics, including movement into the embryo, recycling, and fission.

In our analysis of whether endocytosis was affected in ARX-2–depleted embryos, we found membrane aggregates near the plasma membrane of *arx-2* RNAi-treated embryos (Figure 3D, arrowheads). Such aggregates were not observed as frequently in the controls (Figure 3D). We observed, on average, fewer than three cytoplasmic aggregates per embryo that were >5.98 μm^2 at the PN meeting time point in control embryos (n = 5 embryos). However, in *arx-2* RNAi-treated embryos there were, on average, more than six aggregates >5.98 μm^2 observed at PN meeting (n = 7 embryos). The average size of the larger aggregates in control embryos was 11.4 μm^2, as compared with 13.9 μm^2 in the *arx-2* RNAi-treated embryos. Similar structures could be detected in *arx-2* RNAi-treated embryos expressing GFP-tagged EEA-1(2xFYVE) (Figure 3E), a marker for early endosomes (Andrews and Ahringer, 2007). Therefore we sought to determine whether there were defects at other stages of the endocytic pathway. To determine the nature of the aggregates observed in the FM1-43–labeled embryos, we labeled embryos expressing GFP–EEA-1(2xFYVE) with the fluorescent membrane dye FM4-64. In control embryos at PN meeting, we could detect examples of dye-labeled cytoplasmic "vesicles" that nearly overlapped with GFP–EEA-1(2XFYVE) foci (Supplemental Figure S4B). Similar to the control embryos labeled with FM1-43, few large aggregates were detected in the control embryos labeled

RNAi-treated embryos expressing GFP–PAR-2. (D) Percentage of total cortical area occupied by GFP–PAR-2 was quantified at time points indicated. Results are the mean ± SEM. PN meeting, $p = 0.0029$; PN meeting + 1:00, $p = 0.0019$; PN meeting + 4:00, $p = 0.0037$ (Welch's *t* test, wild-type, n = 5 embryos; *arx-2* RNAi, n = 5 embryos). (E) Cortical Z-series projections of embryos expressing GFP–CDC-42 and GFP–PAR-6. (F) Percentage of total cortical area occupied by GFP–CDC-42 foci was quantified at time points indicated. Results are the mean ± SEM. PN meeting, $p = 0.0448$; PN meeting + 4:00, $p = 1.85 \times 10^{-4}$ (Welch's *t* test, wild-type, n = 7 embryos; *arx-2* RNAi, n = 7 embryos). (G) Cortical Z-series projections of embryos expressing GFP–PAR-6. (H) Percentage of total cortical area occupied by GFP–PAR-6 was quantified at time points indicated. Results are the mean ± SEM. PN meeting + 1:00, $p = 0.0303$ (Welch's *t* test, wild-type, n = 6 embryos; *arx-2* RNAi, n = 6 embryos). (I) Images of single cortical focal plane of control and (J) *arx-2* RNAi-treated embryos expressing GFP–PAR-6 and moe-mCherry. Dotted boxes indicate the area highlighted in the cropped time series (below). Blue arrowheads indicate examples of colocalized or partially colocalized GFP–PAR-6 and moe-mCherry foci. The cropped images are every 10 s from 0:40 s before PN meeting through 0:50 s after PN meeting. Times are in min:s and are relative to PN meeting, 0:00. Asterisks indicate level of significance for compared data. *$p < 0.05$, **$p < 0.01$, ***$p < 0.001$. Scale bar, 20 μm. See also Supplemental Figure S1 for disruption of WAVE/SCAR effects on moe-GFP foci formation.

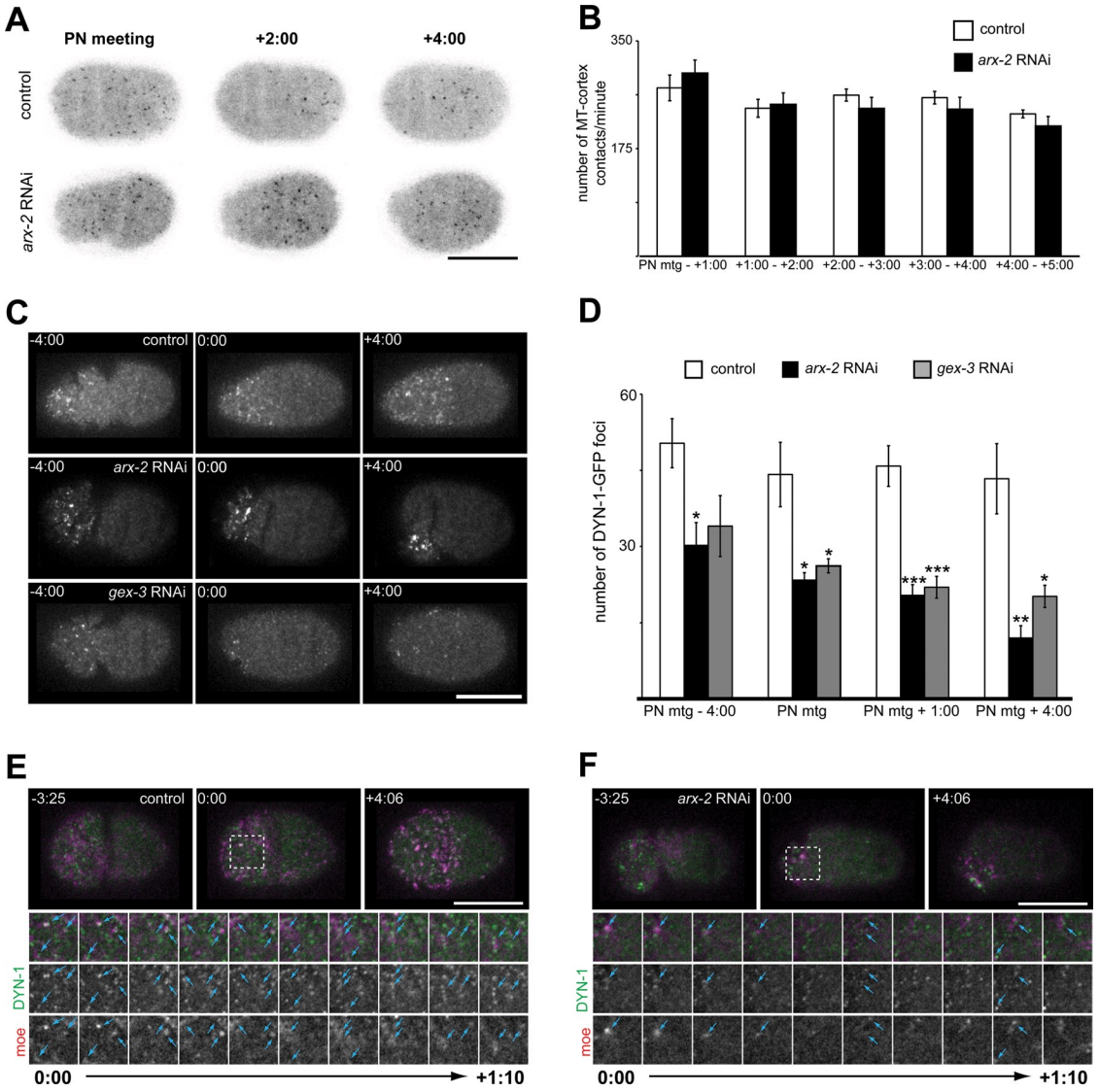

FIGURE 2: ARX-2 affects endocytic protein organization but not microtubule contacts with cortex. (A) Single cortical focal plane of control and *arx-2* RNAi-treated embryos expressing EBP-2–GFP. (B) Graph of the number of EBP-2–GFP foci detected at the cortex each minute. The number of foci at the cortex were counted every 5 s and summed to determine the number of contacts per minute. PN meeting to 1:00, p = 0.4395; 1:00–2:00, p = 0.8011; 2:00–3:00, p = 0.3159; 3:00–4:00, p = 0.4105; 4:00–5:00, p = 0.2760. n = 7 embryos for control and *arx-2* RNAi-treated embryos at all time points. All p values calculated using Welch's *t* test. (C) Cortical projections of control and *arx-2* RNAi- or *gex-3* RNAi-treated embryos expressing DYN-1–GFP. (D) Quantification of the number of anterior cortical DYN-1–GFP foci in wild-type/control, *arx-2*, and *gex-3* RNAi. *arx-2* RNAi vs. control p values are as follows: PN meeting – 4:00, p = 0.014; PN meeting, p = 0.021; PN meeting + 1:00, p = 0.0006; PN meeting + 4:00, p = 0.0049. WT, n = 6 embryos; *arx-2* RNAi, n = 5 embryos. *gex-3* RNAi vs. control p values are as follows: PN meeting – 4:00, p = 0.0662; PN meeting, p = 0.036; PN meeting + 1:00, p = 0.00095; PN meeting + 4:00, p = 0.019. WT, n = 6 embryos; *gex-3* RNAi, n = 5 embryos. Results are the mean ± SEM (E) Single cortical images of wild-type and (F) ARX-2–depleted embryos expressing DYN-1–GFP and moe-mCherry. Dotted box at 0:00 indicates the area highlighted for cropped time series (below). Blue arrowheads indicate examples of colocalized or partially colocalized DYN-1–GFP and moe-mCherry foci. Cropped images are images from every 10 s from PN meeting through 1:10 after PN meeting. For all images, times are in min:s and are relative to PN meeting, 0:00, which is the onset of the maintenance phase. For all graphs, asterisks indicate significance level: *p < 0.05, **p < 0.01, ***p < 0.001. Scale bar, 20 μm. See also Supplemental Figure S3 for *arx-2* RNAi effects on clathrin localization.

with FM4-64 (Supplemental Figure S4B). In the *arx-2* RNAi-treated embryos, we could again detect the larger membrane accumulations in the cytoplasm, and these large, dye-labeled aggregates had multiple GFP-labeled early endosomes associated with them (Supplemental Figure S4B). In *arx-2* RNAi-treated embryos, it also appeared that RAB-5–positive foci were enlarged, similar to our observation in the GFP-EEA-1(2XFYVE)–expressing strain. To determine whether this was the case, we measured the area of RAB-5–labeled endosomes at eight time points from PN meeting through 8:00 after PN meeting. The average areas of the endosomes in controls were initially a bit larger earlier in the cell cycle and then decreased slightly, ranging from 4.6 to 3.7 μm^2 over these

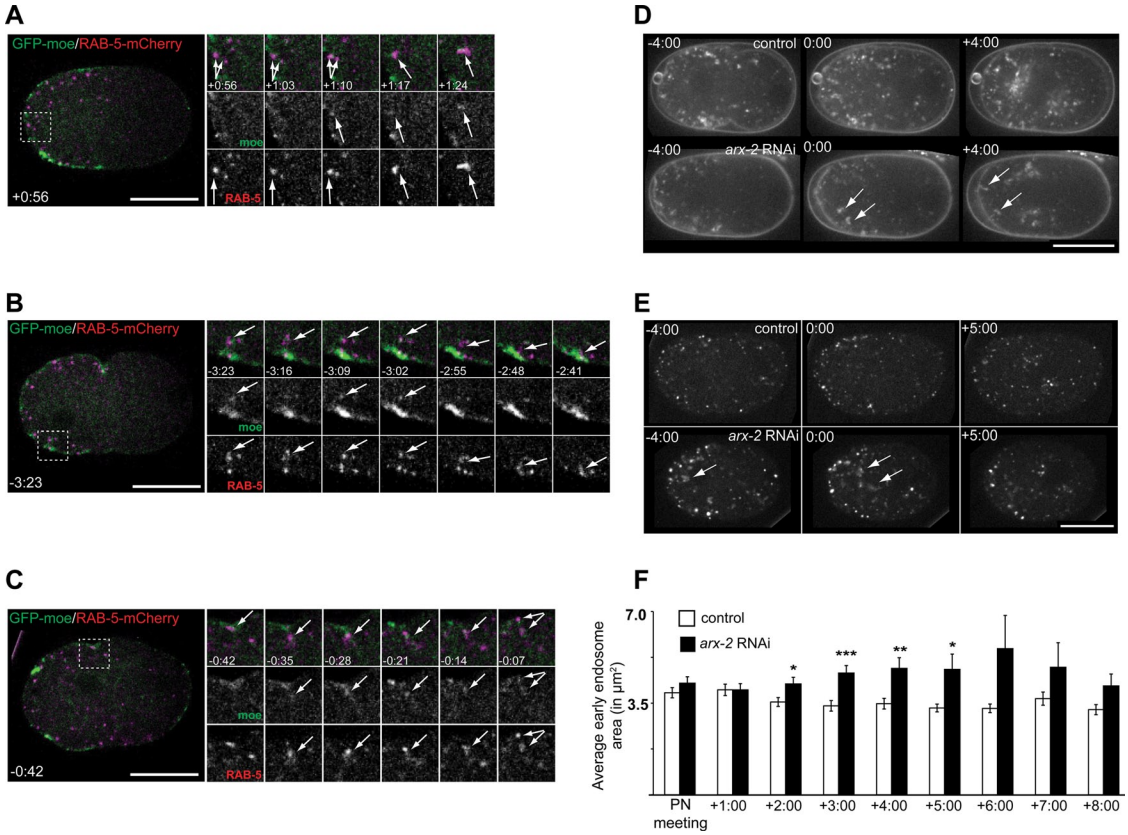

FIGURE 3: Actin associated with early endosomal dynamics. (A–C) Examples of early endosome dynamics in embryos expressing moe-GFP and RAB-5–mCherry. (A) An example of a RAB-5—positive endosome moving away from the plasma membrane along with an accumulation of actin. The dotted box on the full embryo indicates the area that is highlighted in the cropped time series. Arrows indicate the endosome and associated actin exhibiting this movement in the merged and single-channel cropped series. (B) An example of a RAB-5–positive endosome moving back toward the plasma membrane and actin accumulating along with this movement. The dotted box on the full embryo indicates the area highlighted in the cropped time series. Arrows indicate the endosomes and actin foci of interest in the merged and single channels of the cropped series. See also Supplemental Movie S3B. (C) An example of a RAB-5–positive endosome undergoing fission with actin associated just before the division. The dotted box on the full embryo indicates the area highlighted in the cropped time series. Arrows indicate endosomes and actin foci of interest in the merged and single-channel cropped series. See also Supplemental Figure S4 for another example of what appeared to be endosomal fission. Times are in min:s and are relative to PN meeting, 0:00. (D) Time-lapse images of wild-type and *arx-2* RNAi-treated embryos labeled with FM1-43. Arrows indicate examples of membrane aggregates observed. Times are in min:s with respect to PN meeting, 0:00. (E) Time-lapse images of wild-type and *arx-2* RNAi-treated embryos expressing GFP–EEA-1(2xFYVE). Arrows indicate examples of enlarged early endosomes. See also Supplemental Figure S4 for association of GFP–EEA-1 with FM4-64–labeled aggregates in *arx-2* RNAi-treated embryos. (F) Quantification of endosome area at each minute after PN meeting. Times are in min:s with respect to PN meeting, 0:00. p values for control vs. *arx-2* RNAi-treated embryos are as follows: PN meeting, $p = 0.2606$; +1:00, $p = 0.9783$; +2:00, $p = 0.0276$; +3:00, $p = 0.0005$; +4:00, $p = 0.0039$; +5:00, $p = 0.0171$; +6:00, $p = 0.0793$; +7:00, $p = 0.2238$; +8:00, $p = 0.0751$. All p values are calculated using Welch's *t* test. Scale bar, 20 μm.

time points (Figure 3F). In *arx-2* RNAi-treated embryos, the average area was similar to that in controls at PN meeting and at 1:00 after PN meeting (Figure 3F). However, from 2:00 to 5:00 after PN meeting, the average endosome areas were significantly larger than in the controls, >5.0 μm^2, suggesting that ARX-2 affects regulation of early endosome size and possibly trafficking associated with the early endosome. Of interest, the time points at which we observe enlarged endosomes coincides with when we observed greater disruptions in polarity maintenance (Figure 1, C–H). We also examined control and *arx-2* RNAi-treated embryos expressing a GFP-tagged marker for recycling endosomes, RAB-11, and found no obvious effect on the distribution or size of these structures (unpublished data), suggesting that Arp2/3 is playing a specific role in early endosomal regulation. We hypothesize that the efficiency of early endosomal dynamics, such as movement of endosomes away from plasma membrane and endosomal fission, is disrupted upon ARX-2 depletion and that this contributes to the membrane and endosomal aggregates observed.

arx-2 RNAi-formed PAR-6 aggregates are RAB-5 positive

Internalization and recycling of the yeast polarity cue Cdc42p play a key role in maintaining its very distinct "cap" localization, and actin is crucial for this (Marco *et al.*, 2007; Slaughter *et al.*, 2009). Arp2/3 has been reported to play a key role in specific recycling events at the early endosome in higher eukaryotes (Derivery *et al.*, 2009; Puthenveedu *et al.*, 2010). On the basis of the observation that early endosomes were enlarged at the same time that PAR-6 occupied a smaller cortical area and condensed into punctate aggregates in

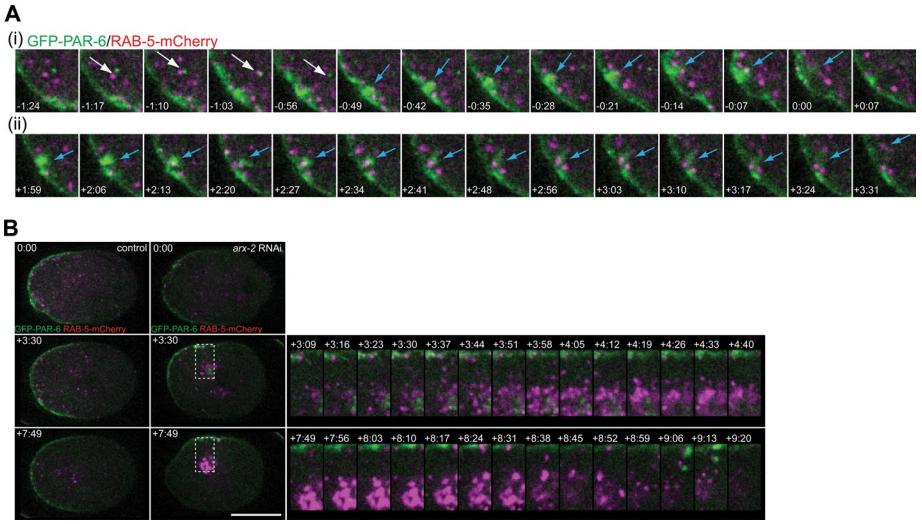

FIGURE 4: PAR-6 accumulates near RAB-5–dense centrosomes in *arx-2* RNAi-treated embryos. (A) Images from control embryos expressing GFP–PAR-6 and RAB-5–mCherry. (i) Cropped time series showing transient movement of PAR-6 cytoplasmic focus with RAB-5–positive endosome (white arrow) and emergence of a large GFP-PAR-6-labeled focus from the cortex into the cytoplasm along with multiple RAB-5–positive foci (blue arrow). (ii) Another example of an accumulation of PAR-6 gradually emerging from the cortex into the cytoplasm with multiple RAB-5–positive endosomes. See also Supplemental Movie S4Aii. (B) Images from control and *arx-2* RNAi-treated embryos expressing GFP–PAR-6 and RAB-5–mCherry. PAR-6 foci accumulate near the centrosome in *arx-2* RNAi-treated embryos much more strongly than in controls. Cropped time series show the accumulation of RAB-5 that coincides with the accumulation of PAR-6 in this area. Finally, a large accumulation of PAR-6 and RAB-5 moves back to the cell periphery during late mitosis (+9:06 to +9:20). Dotted boxes on full embryos indicate the area highlighted in the cropped time series. See also Supplemental Movie S4B control and *arx-2* RNAi. Times are in min:s and are relative to PN meeting. Scale bar, 20 μm.

arx-2 RNAi-treated embryos, we were curious to see whether PAR-6 remained associated with early endosomes aberrantly, possibly due to a failure in trafficking events at the early endosome.

To this end, we generated a strain expressing GFP–PAR-6 and mCherry–RAB-5. In control embryos expressing these constructs, GFP-PAR-6–labeled puncta can be detected in the cytoplasm throughout the cell cycle. We previously reported evidence suggesting these puncta were endocytic, as they frequently moved into the cytoplasm from DYN-1-GFP–rich sites at the cortex (Nakayama *et al.*, 2009). In the cytoplasm of control embryos, the puncta appear to overlap partially with RAB-5–positive endosomes transiently (Figure 4A, white arrow). In a single focal plane, we observed events of this nature six times per embryo, on average. We found that these adjacent/partially overlapped PAR-6– and RAB-5–positive structures could be observed moving together for multiple frames. They typically moved together for ~30 s before separating, but more frequently it seemed that the structures drifted out of the focal plane and could therefore no longer be tracked. Longer associations could be detected as well, ranging from 70 to 98 s, although typically only one of these long associations was observed per embryo imaged in a single focal plane. Overall, 55% of the cytoplasmic PAR-6 structures were associated with RAB-5–positive endosomes for multiple time points, and these associations were rarely detected at the centrosomes. Of interest, 54.5% of the cytoplasmic PAR-6 puncta that we observed not associated with RAB-5–positive endosomes were observed in the posterior region of the cell (n = 5 embryos).

We also observed RAB-5–positive endosomes associated with the movement of large PAR-6 puncta into the cytoplasm (Figure 4A, i and ii, blue arrows; see also Supplemental Movie Figure 4Aii). In the *arx-2* RNAi-treated embryos, centrosomal aggregates of GFP–PAR-6 can be detected when the pronuclei begin to move to the center of the embryo after meeting (Figure 4B; see also Supplemental Movie S4B control and *arx-2* RNAi). These accumulations are much larger than what is observed in the control embryos and appear to remain associated with RAB-5 near the centrosome (Figure 4B, +3:09 to +4:40). During mitosis, the RAB-5– and PAR-6–positive aggregates move rapidly toward the cortex (Figure 4B, +7:49 to +9:20). During the maintenance phase, there also appears to be an intense localization of RAB-5 that remains associated with the centrosome more than that observed in controls (Figure 4B). These data suggest that Arp2/3-mediated actin dynamics affects the endocytic trafficking dynamics of PAR-6 and early endosomes, possibly by regulating the normally rapid recycling of PAR-6 from early endosomal compartments back to the cortex to stabilize the size of the anterior domain.

DISCUSSION

Our observation of disruption in PAR asymmetry and actin dynamics during polarity maintenance phase is similar to recently reported data (Xiong *et al.*, 2011). The ratio of posterior to anterior PAR-2 fluorescence intensity was significantly decreased in *arx-2* RNAi-treated embryos, which matches our observation that PAR-2 occupies a significantly greater cortical area. We also found a slight decrease in cortical area occupied by PAR-6 that was significant 1:00 after PN meeting, as well as residual GFP–PAR-6 foci near the cortex later in the maintenance phase. This suggests that there is, indeed, some disruption of PAR-6 dynamics upon *arx-2* depletion. We suggest that this difference in observation might be due to examining the ratio of fluorescence intensities at the mid-focal plane as opposed to measuring the size of the PAR domains in cortical images, as we did in this study. We also report that CDC-42 accumulates at the cortex during the maintenance phase when Arp2/3 dynamics is disrupted. Taken together, both studies clearly indicate a role for Arp2/3-mediated actin dynamics in the stabilization of PAR asymmetry during the maintenance phase.

These studies also differ in that we did not observe the same defects in microtubules as Xiong *et al.* (2011). We observed that the number of microtubule plus ends that made contact with the cortex was similar in *arx-2* RNAi-treated embryos and controls. These data suggest that although the centrosomes may be smaller (Xiong *et al.*, 2011), the ability of microtubules to contact the cortex is not affected when Arp2/3 function is disrupted. However, the most apparent difference in our study is our characterization of the dynamics of endocytic proteins and compartments in association with actin dynamics. We showed that depletion of ARX-2 leads to significant disruptions in the recruitment and organization of different markers of the endocytic machinery at the cortex. Although we did not observe changes in amount or asymmetry of endocytosis, it is possible that in decreasing the levels of ARX-2 the overall efficiency of the endocytic pathway is reduced. We hypothesize that this inefficiency then leads to the disruption of PAR asymmetry. When Arp2/3 function is altered, we found that early endosome dynamics is disrupted, and

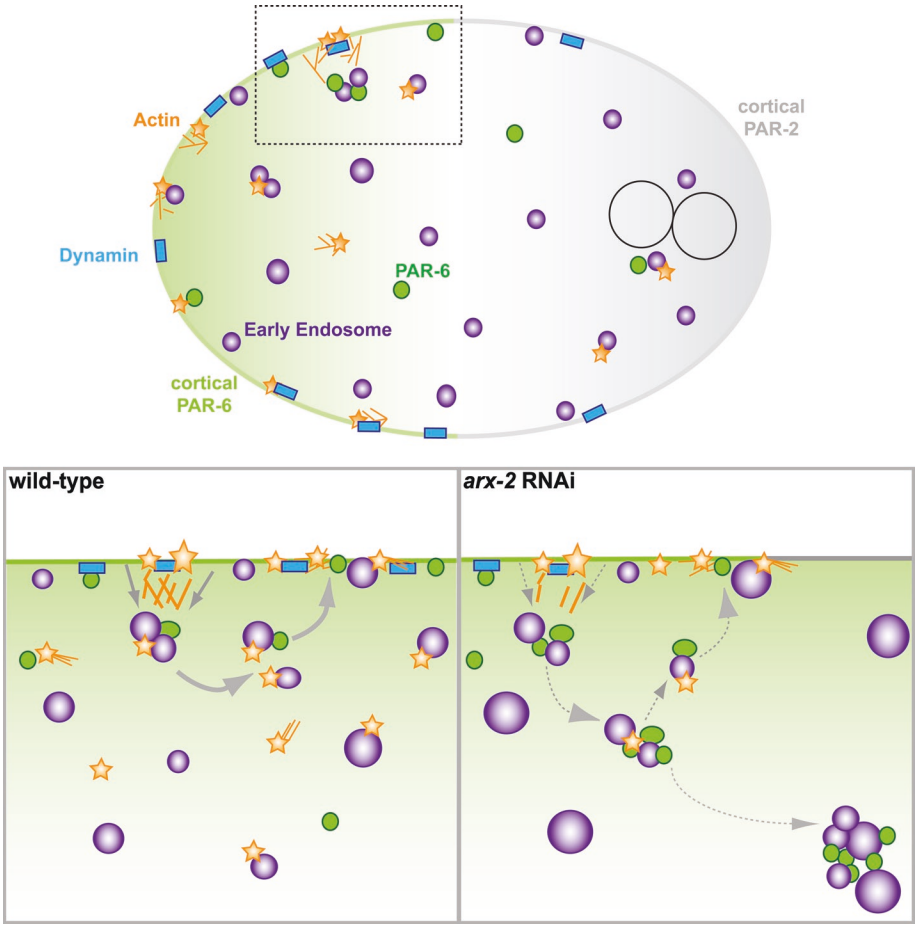

FIGURE 5: Model for the maintenance of PAR asymmetry. Model proposed based on our observations and those of previous work. In wild-type embryos during the maintenance phase, actin (yellow stars) and dynamin (blue squares) associate at the cortex. Dynamin promotes the internalization of PAR-6 (green). PAR-6 associates with early endosomes (purple circles), which in some instances are associated with cytoplasmic actin foci. These actin foci appear to help regulate endosomal behaviors, such as endosome scission or recycling. Cytoplasmic puncta of PAR-6 can then be rapidly recycled back to the cortex if necessary or possibly move on to other endocytic compartments. On disruption of Arp2 levels, PAR-6 may not be internalized as efficiently, as indicated by the reduction in dynamin sites at the cortex. Early endosomes are significantly larger, possibly due to defects in endosome scission. PAR-6 cytoplasmic accumulations are detected in association with large early endosome aggregates. Owing to the aberrant accumulation of cytoplasmic PAR-6 in association with early endosomes, the balance between cortically localized PAR-6 and PAR-2 (gray) is disrupted.

cytoplasmic GFP-PAR-6 aggregates accumulate near the anterior centrosome at the times at which PAR-6 occupies a smaller cortical area. These PAR-6 accumulations are associated with larger RAB-5–positive endosomes, leading us to conclude that Arp2/3-mediated actin dynamics participates in the rapid recycling of internalized PAR-6 back to the cortex during maintenance phase. Typically Rab4 is associated with the rapid recycling of cargo from the early endosome (Yudowski *et al.*, 2009); however, a Rab4 homologue has not been identified in *C. elegans* (Grant and Hirsh, 1999). Given that we observe RAB-5–positive foci moving from the cytoplasm back to the plasma membrane (Figure 3B), it is possible that RAB-5 is taking on a recycling role as well.

The involvement of actin in the endocytic maintenance of polarity cues has been discussed in terms of many experimental systems (Ayscough, 2000; Marco *et al.*, 2007; Georgiou *et al.*, 2008; Leibfried *et al.*, 2008; Robertson *et al.*, 2009; Slaughter *et al.*, 2009; Harris and Tepass, 2010; Shivas *et al.*, 2010). Although the role of actin in maintaining single-cell polarity via localized recycling of polarity cues in yeast has been discussed (Irazoqui *et al.*, 2005; Slaughter *et al.*, 2009; Yamamoto *et al.*, 2010), it has not been reported widely in higher eukaryotic systems. Defects in the rapid recycling of PAR-6 from the early endosome seem to be the most likely cause of disruption in PAR cortical localization and PAR-6 cytoplasmic accumulation, but we have not ruled out the possibility that inefficiencies at earlier stages of endocytosis could lead to the problems in recycling as well. Actin regulators have been reported to play a role in vesicle uncoating (Kaksonen *et al.*, 2005; Galletta *et al.*, 2008; Galletta and Cooper, 2009). Defects in cargo recycling have been attributed to failures in efficient vesicle uncoating (Kim *et al.*, 2002; Galletta and Cooper, 2009). Such a defect might explain the aberrant accumulations of PAR-6 foci, CDC-42, and clathrin near the cortex and the accumulation of PAR-6 and RAB-5 at the centrosomes.

Why would a cell internalize proteins only to recycle them soon after? We hypothesize that the mechanism described here acts to dynamically correct the size of the established PAR domains before the onset of mitosis, when the PAR proteins have been shown to diffuse rapidly (Goehring *et al.*, 2011). Models in yeast suggest that a balance among endocytosis, recycling, and diffusion is key for stabilizing asymmetrically localized factors such as Cdc42p (Marco *et al.*, 2007; Slaughter *et al.*, 2009), and actin plays a central role in these processes (Ayscough, 2000; Irazoqui *et al.*, 2005; Marco *et al.*, 2007; Slaughter *et al.*, 2009; Harris and Tepass, 2010; Orlando *et al.*, 2011). In our study, we suggest that we disrupted this balance of mechanisms involved in maintaining the asymmetric localization of polarity cues by disrupting recycling and possibly reducing the efficiency of endocytosis. We propose a model in which the actin foci observed at the cortex during the maintenance phase form in an Arp2/3-dependent manner and play a role in the organization of the endocytic machinery at the cortex (Figure 5). They may also promote the efficiency of endocytosis, endosome movement away from the plasma membrane, and vesicle uncoating here. In the cytoplasm, ARX-2–dependent actin foci colocalize with some RAB-5–positive early endosomes. Under conditions in which ARX-2 levels are reduced, endosomal dynamics such as endosome fission and recycling of PAR-6 are disrupted, causing aberrant trafficking to the centrosomal area and destabilization in the maintenance of cortically localized polarity cues.

In conclusion, the data presented here suggest a mechanism in which Arp2/3-mediated actin dynamics play a key role in regulating events during the maintenance phase, including endocytic recycling dynamics and organization. The ability of this pathway to function efficiently reinforces the established PAR-6 localization and overall PAR asymmetry before the embryo enters mitosis. Future

experiments using more biochemical methods to determine the membrane fractions with which the PAR proteins and CDC-42 are associating will enhance our understanding of this process. It also remains unclear how the anterior PAR complex is linked to the plasma membrane in this system and what role CDC-42 plays in this. Determining this connection could answer the question of how these factors are targeted to their appropriate location, which would greatly clarify our model of how exactly asymmetrically localized proteins are stabilized in a dynamic environment.

EXPERIMENTAL PROCEDURES

GFP fusions

The following transgenic lines were used: N2, JJ1579 (GFP–PAR-6; Munro *et al.*, 2004), TH129 (GFP–PAR-2; Schonegg *et al.*, 2007), SA131 (GFP–CDC-42; Motegi and Sugimoto, 2006), PF100 (GFP-moe; Motegi *et al.*, 2006), MAD3 (DYN-1b^{FL}–GFP; Nakayama *et al.*, 2009), MAD21 (DYN-1–GFP × mCherry–PAR-6; Nakayama *et al.*, 2009), JA1403 (GFP–EEA-1(2X FYVE; Andrews and Ahringer, 2007), and TH66 (EBP-2–GFP; Srayko *et al.*, 2005). All strains were maintained at room temperature (22°C).

Strains generated in this work: MAD36 (moe-mCherry; this work), MAD45 (moe-mCherry × DYN-1–GFP; this work), MAD43 (moe-GFP × mCherry–RAB-5; this work; Audhya *et al.*, 2007), MAD53 (GFP–PAR-6 × moe-mCherry; Munro *et al.*, 2004; this work), and MAD60 (GFP–PAR-6 × RAB-5–mCherry; Munro *et al.*, 2004; Audhya *et al.*, 2007).

To generate strains that express moe-mCherry, the moe fragment was amplified from a pFJ1-based vector, pMOE (Velarde *et al.*, 2007), and then inserted into the *Spe*I site of pAA64 (McNally *et al.*, 2006). The primers used for amplification of moe are sense primer, 5′-AGACCACATGGTCCTTCTTGAG-3′, and antisense primer, 5′-AAAGAGAGGGGGTGAGTGGAT-3′. The resulting vector contains a 5.7-kb genomic fragment of *unc-119* and a fragment coding the actin-binding domain of moesin fused to N-terminus of GFP; GFP fusions are driven by the *pie-1* promoter. This vector (pJMS06 moe-mCherry in pAA64) was bombarded into the *unc-119* strain, and movers were isolated and assayed for fluorescence.

RNA interference

For the *arx-2* fRNAi experiments, the *arx-2* gene was obtained from the Ahringer RNAi feeding library (Kamath *et al.*, 2003). Knockdown of gene function was performed using RNA feeding methods (Kamath and Ahringer, 2003). The temperature for fRNAi treatments was 25°C for 22–30 h.

Live imaging and analysis of GFP fluorescence

Embryos were dissected in egg salt buffer (118 mM NaCl, 40 mM KCl, 3.4 mM $CaCl_2$, 3.4 mM $MgCl_2$, 5 mM 4-(2-hydroxyethyl)-1-piperazineethanesulfonic acid, pH 7.2; Munro *et al.*, 2004) and mounted on a 2% agarose pad in egg buffer, and a 22 × 22 mm coverslip was placed on top and sealed with Vaseline. GFP time-lapse video images were captured using a motorized microscope (Axioplan II; Carl Zeiss, Jena, Germany) equipped with a spinning disk confocal scan head (QLC100; VisiTech, Sunderland, United Kingdom). The motorized filter turret and focus, external shutters, and a 12-bit camera (Orca ER; Hamamatsu, Hamamatsu, Japan) were controlled using OpenLab software (Improvision, PerkinElmer, Waltham, MA). For cortical time-lapse imaging, we collected a Z-series of 2 frames per time point, and converted each Z-series into a single image by maximum projection. Image processing was done with Photoshop (Adobe, San Jose, CA) or ImageJ software (National Institutes of Health, Bethesda, MD).

FM dye imaging

For wild-type membrane dynamics, embryos were mounted on uncoated coverslips in hanging drops containing 1 μg/ml FM1-43 (Molecular Probes, Invitrogen, Carlsbad, CA) in egg salts. Fluorescence was captured with a 488-nm argon laser and 520-nm emission filter.

Quantification

For cortical area occupied, background fluorescent signals other than the major foci were removed by setting a threshold value that minimized background fluorescence in regions devoid of GFP signal or foci. The areas of fluorescence above the threshold value in each anterior and posterior region were measured using the Percent Area measurement in the ImageJ measurement tools. To quantify the number of microtubule contacts made with the cortex, the embryos expressing EBP-2–GFP were imaged every 5 s. The number of foci at the cortex were counted manually every 5 s for a total of 60 s. The numbers of foci at each time point were summed to obtain the number of contacts/minute. To quantify the number of DYN-1–GFP foci at the cortex, background fluorescence was subtracted in each cortical Z-series projection using the ImageJ Subtract Background function. A threshold was set such that the DYN-1–GFP foci were highlighted, and background fluorescence that remained was minimally detected. The foci were analyzed using Analyze Particles in ImageJ with a cutoff of 5 pixels^2. To quantify the endosome area, a threshold was set so that all of the FM1-43–labeled or RAB-5–labeled endosomes in the focal plane were highlighted and the background fluorescence recognized was minimal. Using the Analyze Particles function in ImageJ, we measured the area of the highlighted endosomes by setting a cutoff of 30 pixels^2 for FM1-43 to determine how frequently larger-than-average endosomes were observed in controls and *arx-2* RNAi-treated embryos and 10 pixels^2 for RAB-5 to determine the average endosome size at each time point.

Statistical analysis

The quantified values were compared between wild-type/control and *arx-2* fRNAi-treated embryos. An *F* test was used to compare the variance between subjects before applying the *t* test. When the variance was equal, Student's *t* test (two tails) was used to analyze the difference between wild-type and *arx-2* fRNAi-treated embryos. When the variances were unequal, Welch's *t* test was used. The statistical tests were done using Excel (Microsoft, Redmond, WA). $p < 0.05$ was considered statistically significant.

ACKNOWLEDGMENTS

We thank A. Audhya, B. Goldstein, B. Grant, A. Hyman, E. Munro, F. Piano, M. Soto, and N. Velarde for the generous gift of reagents and advice. We thank D. S. Poole for assistance and guidance. Some of the strains used in this study were kindly provided by the *Caenorhabditis* Genetics Center, which is funded by the National Institutes of Health National Center for Research Resources. This work was supported by National Institutes of Health K01 Research Career Development Award K01HL092585 and the Louis and Elsa Thomsen Wisconsin Distinguished Graduate Fellowship.

REFERENCES

Aceto D, Beers M, Kemphues KJ (2006). Interaction of PAR-6 with CDC-42 is required for maintenance but not establishment of PAR asymmetry in *C. elegans*. Dev Biol 299, 386–397.

Ai E, Poole DS, Skop AR (2011). Long astral microtubules and RACK-1 stabilize polarity domains during maintenance phase in *Caenorhabditis elegans* embryos. PLoS ONE 6, e19020.

Andrews R, Ahringer J (2007). Asymmetry of early endosome distribution in *C. elegans* embryos. PLoS ONE 2, e493.

Audhya A, Desai A, Oegema K (2007). A role for Rab5 in structuring the endoplasmic reticulum. J Cell Biol 178, 43–56.
Ayscough KR (2000). Endocytosis and the development of cell polarity in yeast require a dynamic F-actin cytoskeleton. Curr Biol 10, 1587–1590.
Cai Y, Yu F, Lin S, Chia W, Yang X (2003). Apical complex genes control mitotic spindle geometry and relative size of daughter cells in *Drosophila* neuroblast and pI asymmetric divisions. Cell 112, 51–62.
Cowan CR, Hyman AA (2007). Acto-myosin reorganization and PAR polarity in *C. elegans*. Development 134, 1035–1043.
Cuenca AA, Schetter A, Aceto D, Kemphues K, Seydoux G (2003). Polarization of the *C. elegans* zygote proceeds via distinct establishment and maintenance phases. Development 130, 1255–1265.
Derivery E, Sousa C, Gautier JJ, Lombard B, Loew D, Gautreau A (2009). The Arp2/3 activator WASH controls the fission of endosomes through a large multiprotein complex. Dev Cell 17, 712–723.
Ferguson SM, De Camilli P (2012). Dynamin, a membrane-remodelling GTPase. Nat Rev 13, 75–88.
Galletta BJ, Chuang DY, Cooper JA (2008). Distinct roles for Arp2/3 regulators in actin assembly and endocytosis. PLoS Biol 6, e1.
Galletta BJ, Cooper JA (2009). Actin and endocytosis: mechanisms and phylogeny. Curr Opin Cell Biol 21, 20–27.
Georgiou M, Marinari E, Burden J, Baum B (2008). Cdc42, Par6, and aPKC regulate Arp2/3-mediated endocytosis to control local adherens junction stability. Curr Biol 18, 1631–1638.
Goehring NW, Hoege C, Grill SW, Hyman AA (2011). PAR proteins diffuse freely across the anterior-posterior boundary in polarized *C. elegans* embryos. J Cell Biol 193, 583–594.
Goldstein B, Macara IG (2007). The par proteins: fundamental players in animal cell polarization. Dev Cell 13, 609–622.
Goley ED, Welch MD (2006). The ARP2/3 complex: an actin nucleator comes of age. Nat Rev 7, 713–726.
Grant B, Hirsh D (1999). Receptor-mediated endocytosis in the *Caenorhabditis elegans* oocyte. Mol Biol Cell 10, 4311–4326.
Harris KP, Tepass U (2010). Cdc42 and vesicle trafficking in polarized cells. Traffic 11, 1272–1279.
Irazoqui JE, Howell AS, Theesfeld CL, Lew DJ (2005). Opposing roles for actin in Cdc42p polarization. Mol Biol Cell 16, 1296–1304.
Kaksonen M, Toret CP, Drubin DG (2005). A modular design for the clathrin- and actin-mediated endocytosis machinery. Cell 123, 305–320.
Kaksonen M, Toret CP, Drubin DG (2006). Harnessing actin dynamics for clathrin-mediated endocytosis. Nat Rev 7, 404–414.
Kamath RS, Ahringer J (2003). Genome-wide RNAi screening in *Caenorhabditis elegans*. Methods 30, 313–321.
Kamath RS *et al*. (2003). Systematic functional analysis of the *Caenorhabditis elegans* genome using RNAi. Nature 421, 231–237.
Kim WT, Chang S, Daniell L, Cremona O, Di Paolo G, De Camilli P (2002). Delayed reentry of recycling vesicles into the fusion-competent synaptic vesicle pool in synaptojanin 1 knockout mice. Proc Natl Acad Sci USA 99, 17143–17148.
Krueger EW, Orth JD, Cao H, McNiven MA (2003). A dynamin-cortactin-Arp2/3 complex mediates actin reorganization in growth factor-stimulated cells. Mol Biol Cell 14, 1085–1096.
Lanzetti L (2007). Actin in membrane trafficking. Curr Opin Cell Biol 19, 453–458.
Lee E, De Camilli P (2002). Dynamin at actin tails. Proc Natl Acad Sci USA 99, 161–166.
Leibfried A, Fricke R, Morgan MJ, Bogdan S, Bellaiche Y (2008). *Drosophila* Cip4 and WASp define a branch of the Cdc42-Par6-aPKC pathway regulating E-cadherin endocytosis. Curr Biol 18, 1639–1648.
Marco E, Wedlich-Soldner R, Li R, Altschuler SJ, Wu LF (2007). Endocytosis optimizes the dynamic localization of membrane proteins that regulate cortical polarity. Cell 129, 411–422.
McNally K, Audhya A, Oegema K, McNally FJ (2006). Katanin controls mitotic and meiotic spindle length. J Cell Biol 175, 881–891.
McNiven MA, Kim L, Krueger EW, Orth JD, Cao H, Wong TW (2000). Regulated interactions between dynamin and the actin-binding protein cortactin modulate cell shape. J Cell Biol 151, 187–198.
Merrifield CJ, Feldman ME, Wan L, Almers W (2002). Imaging actin and dynamin recruitment during invagination of single clathrin-coated pits. Nat Cell Biol 4, 691–698.
Merrifield CJ, Moss SE, Ballestrem C, Imhof BA, Giese G, Wunderlich I, Almers W (1999). Endocytic vesicles move at the tips of actin tails in cultured mast cells. Nat Cell Biol 1, 72–74.
Motegi F, Sugimoto A (2006). Sequential functioning of the ECT-2 RhoGEF, RHO-1 and CDC-42 establishes cell polarity in *Caenorhabditis elegans* embryos. Nat Cell Biol 8, 978–985.
Motegi F, Velarde NV, Piano F, Sugimoto A (2006). Two phases of astral microtubule activity during cytokinesis in *C. elegans* embryos. Dev Cell 10, 509–520.
Munro E, Nance J, Priess JR (2004). Cortical flows powered by asymmetrical contraction transport PAR proteins to establish and maintain anterior-posterior polarity in the early *C. elegans* embryo. Dev Cell 7, 413–424.
Nakayama Y, Shivas JM, Poole DS, Squirrell JM, Kulkoski JM, Schleede JB, Skop AR (2009). Dynamin participates in the maintenance of anterior polarity in the *Caenorhabditis elegans* embryo. Dev Cell 16, 889–900.
Orlando K, Sun X, Zhang J, Lu T, Yokomizo L, Wang P, Guo W (2011). Exo-endocytic trafficking and the septin-based diffusion barrier are required for the maintenance of Cdc42p polarization during budding yeast asymmetric growth. Mol Biol Cell 22, 624–633.
Patel FB, Bernadskaya YY, Chen E, Jobanputra A, Pooladi Z, Freeman KL, Gally C, Mohler WA, Soto MC (2008). The WAVE/SCAR complex promotes polarized cell movements and actin enrichment in epithelia during *C. elegans* embryogenesis. Dev Biol 324, 297–309.
Puthenveedu MA, Lauffer B, Temkin P, Vistein R, Carlton P, Thorn K, Taunton J, Weiner OD, Parton RG, von Zastrow M (2010). Sequence-dependent sorting of recycling proteins by actin-stabilized endosomal microdomains. Cell 143, 761–773.
Ridley AJ (2006). Rho GTPases and actin dynamics in membrane protrusions and vesicle trafficking. Trends Cell Biol 16, 522–529.
Robertson AS, Smythe E, Ayscough KR (2009). Functions of actin in endocytosis. Cell Mol Life Sci 66, 2049–2065.
Sato M, Sato K, Fonarev P, Huang CJ, Liou W, Grant BD (2005). *Caenorhabditis elegans* RME-6 is a novel regulator of RAB-5 at the clathrin-coated pit. Nat Cell Biol 7, 559–569.
Schafer DA (2002). Coupling actin dynamics and membrane dynamics during endocytosis. Curr Opin Cell Biol 14, 76–81.
Schafer DA (2004). Regulating actin dynamics at membranes: a focus on dynamin. Traffic 5, 463–469.
Schenk C, Bringmann H, Hyman AA, Cowan CR (2010). Cortical domain correction repositions the polarity boundary to match the cytokinesis furrow in *C. elegans* embryos. Development 137, 1743–1753.
Schonegg S, Constantinescu AT, Hoege C, Hyman AA (2007). The Rho GTPase-activating proteins RGA-3 and RGA-4 are required to set the initial size of PAR domains in *Caenorhabditis elegans* one-cell embryos. Proc Natl Acad Sci USA 104, 14976–14981.
Severson AF, Bowerman B (2003). Myosin and the PAR proteins polarize microfilament-dependent forces that shape and position mitotic spindles in *Caenorhabditis elegans*. J Cell Biol 161, 21–26.
Shivas JM, Morrison HA, Bilder D, Skop AR (2010). Polarity and endocytosis: reciprocal regulation. Trends Cell Biol 20, 445–452.
Siegrist SE, Doe CQ (2007). Microtubule-induced cortical cell polarity. Genes Dev 21, 483–496.
Slaughter BD, Das A, Schwartz JW, Rubinstein B, Li R (2009). Dual modes of cdc42 recycling fine-tune polarized morphogenesis. Dev Cell 17, 823–835.
Smythe E, Ayscough KR (2006). Actin regulation in endocytosis. J Cell Sci 119, 4589–4598.
Soto MC, Qadota H, Kasuya K, Inoue M, Tsuboi D, Mello CC, Kaibuchi K (2002). The GEX-2 and GEX-3 proteins are required for tissue morphogenesis and cell migrations in *C. elegans*. Genes Dev 16, 620–632.
Srayko M, Kaya A, Stamford J, Hyman AA (2005). Identification and characterization of factors required for microtubule growth and nucleation in the early *C. elegans* embryo. Dev Cell 9, 223–236.
Taunton J (2001). Actin filament nucleation by endosomes, lysosomes and secretory vesicles. Curr Opin Cell Biol 13, 85–91.
Taunton J, Rowning BA, Coughlin ML, Wu M, Moon RT, Mitchison TJ, Larabell CA (2000). Actin-dependent propulsion of endosomes and lysosomes by recruitment of N-WASP. J Cell Biol 148, 519–530.
Velarde N, Gunsalus KC, Piano F (2007). Diverse roles of actin in *C. elegans* early embryogenesis. BMC Dev Biol 7, 142.
Xiong H, Mohler WA, Soto MC (2011). The branched actin nucleator Arp2/3 promotes nuclear migrations and cell polarity in the *C. elegans* zygote. Dev Biol 357, 356–369.
Yamamoto T, Mochida J, Kadota J, Takeda M, Bi E, Tanaka K (2010). Initial polarized bud growth by endocytic recycling in the absence of actin cable-dependent vesicle transport in yeast. Mol Biol Cell 21, 1237–1252.
Yarar D, Waterman-Storer CM, Schmid SL (2005). A dynamic actin cytoskeleton functions at multiple stages of clathrin-mediated endocytosis. Mol Biol Cell 16, 964–975.
Yudowski GA, Puthenveedu MA, Henry AG, von Zastrow M (2009). Cargo-mediated regulation of a rapid Rab4-dependent recycling pathway. Mol Biol Cell 20, 2774–2784.